NASA TECHNICAL NOTE

NASA TN D-5281

c. 1

NASA TN D-5281

DESIGN OF AN ELECTRONICALLY SCANNED STAR SENSOR WITH DIGITAL OUTPUT

by Aaron J. Ostroff and K. C. Romanczyk

Langley Research Center
Langley Station, Hampton, Va.

NATIONAL AERONAUTICS AND SPACE ADMINISTRATION • WASHINGTON, D. C. • JUNE 1969

DESIGN OF AN ELECTRONICALLY SCANNED STAR SENSOR WITH DIGITAL OUTPUT

By Aaron J. Ostroff and K. C. Romanczyk

Langley Research Center
Langley Station, Hampton, Va.

NATIONAL AERONAUTICS AND SPACE ADMINISTRATION

For sale by the Clearinghouse for Federal Scientific and Technical Information
Springfield, Virginia 22151 – CFSTI price $3.00

DESIGN OF AN ELECTRONICALLY SCANNED STAR SENSOR WITH DIGITAL OUTPUT

By Aaron J. Ostroff and K. C. Romanczyk
Langley Research Center

SUMMARY

A technique for detecting the change in position of a star on the focal plane of a telescope is described. In this technique an image dissector is used to scan the focal plane and to generate position information. Both theoretical and experimental data are presented.

The theoretical analysis contains information on signal-to-noise ratio and relationships between star magnitude, system stability, and sweep frequency. Statistical methods are included for determining the standard deviation for detecting any signal pulse, and for calculating the error involved for one or for several measuring periods.

The experimental data contain information on the variation of system stability with star magnitude as functions of sweep frequency, threshold level, and averaged data. All testing is for a simulated 3-meter-diameter telescope operating at f/100. Results show that for a triangular sweep frequency of 100 hertz and a star magnitude of +10, the system is stable to within ±26.4 nanoradians. This represents a system signal-to-noise ratio of 370. Other results indicate that the system is linear within ±0.6 percent of best straight line over a total field of view of ±9.76 milliradians.

INTRODUCTION

The NASA is currently investigating the feasibility of operating a large orbiting astronomical telescope. This class of telescope will require the use of stars within the main optics field of view for guidance. A recently completed study (ref. 1) of a 3-meter-diameter (120-inch), diffraction-limited telescope concluded that a fine-pointing control system will be needed to stabilize the telescope within ±48.5 nanoradians (±0.01 arc sec). The system would also be required to guide on stars of +10 magnitude or fainter.

As a result of this study, the question arose as to the type of transducer and measuring technique that might be used. Most available sensors work on some variation of the principle of physically dividing the focal plane in the vicinity of a star image into quadrants. When the star image is exactly centered in this region, all quadrants will

have equal intensities. Any angular motion of the optical system will result in unequal intensities which provides the basis for a highly sensitive analog nulling device. An obvious penalty is a very small linear range. A technique was desired that is basically digital for ease of processing, is capable of measuring errors rapidly, has a wide field of view which is easily adjustable, and is linear over the complete range. Furthermore, the measuring technique should be simple.

In order to meet these requirements, a scanning technique using an image dissector tube as the transducer has been investigated. Results of the various experiments are discussed and include several graphs showing system accuracy as a function of star magnitude, scanning frequency, number of measurements averaged, and signal-pulse detection level. Linearity and range are also included.

SYMBOLS

A	image area seen by transducer, normalized to unity
A_l	area of lens
A_p	area of primary
A_s	area obscured by secondary
A_t	usable area of telescope $\left(A_p - A_s\right)$
E	system-stability error
E_r	ratio of system-stability error for any two stars
e	electron charge $\left(1.6 \times 10^{-19} \text{ coulomb}\right)$
F	incoming light intensity
F_r	ratio of light intensity for any two stars
$H_{AO\underline{V}}$	absolute spectral irradiance from zero-magnitude AOV star at 10 700° K without atmospheric filtering effects
H_{ss}	absolute spectral irradiance of star simulator at objective of transducer

I_a	signal current, amperes
K	number of samples
k	statistical value due to electron multiplication
m	star magnitude as seen by transducer when star simulator is at a specified distance
m_1	magnitude of star number 1
m_2	magnitude of star number 2
N	digital output number
n	sample number
P	number of counting periods
p	number of signal pulse in measurement (also used as subscript)
R	scale factor
R_L	resistance of load
R_λ	relative spectral response of transducer
S/N	signal-to-noise ratio
T_s	time required for image to move from just outside of slit to completely within slit
t	any time between zero and T_s
$\bar{t}$	arithmetic average time
t_l	time from center of signal pulse to leading edge at detection time (fig. 5)
t_{mc}	time for measured signal-pulse center

t_n time for any sample number

t_t time from center of signal pulse to trailing edge at detection time (fig. 5)

t_1 time between first two pulses in train

t_2 time between second two pulses in train

t_ϵ difference between measured signal-pulse center and actual signal-pulse center

Δf noise bandwidth, hertz

Δm incremental star magnitude

δt_n deviation from arithmetic average $\left(t_n - \bar{t}\right)$

$\delta t_{\ell n}$ deviation from arithmetic average for leading-edge time

δt_{tn} deviation from arithmetic average for trailing-edge time

λ wavelength of light, micrometer

μ current amplification

ρ correlation coefficient

σ standard deviation

σ_n standard deviation from a number of samples

PRINCIPLES OF OPERATION

Description of Star Sensor

This section contains a description of the transducer operating principles and the measuring techniques used to measure star position.

The transducer is an image dissector, which is a specialized photomultiplier tube. (See fig. 1.) The photocathode emits electrons at a rate proportional to the incident light intensity. The electrons are accelerated through a drift tube and are focused onto a plane containing the defining aperture. The electron image of a star can be moved across the aperture by passing an electrical signal through the magnetic deflection coil. Although

the star image physically remains in one spot on the face of the tube, an electrical sweep signal creates the impression that the image is in constant motion by oscillating the electron image of the star. The path of the electron image is defined by the sweep signal. When the electrons pass through the aperture, a slit in this case, they impinge on a series of dynodes causing electron multiplication. The resulting signal pulse is measured across the anode load resistor and the amplitude is proportional to the incident light intensity.

Measuring Technique

The basic principle of the measuring technique can be seen from figure 2. A triangular sweep signal is shown in the upper half of this figure with the dotted horizontal line indicating the position of the slit relative to the electron image. The idealized electrical pulses in the lower half of the figure occur when the image crosses the slit. The time interval between successive pulses is measured. The difference in the two times $(t_1$ and $t_2)$ is proportional to the distance between the projection of the star image at the anode and the slit. The slit is a perforation in the anode. The sign of the resulting number indicates direction.

The pulse train is processed as shown in figure 3. The signal pulses are first amplified and then filtered. The principal effect of this filter is to lower the noise bandwidth Δf of the system. The leading and trailing edges of the resulting pulses are then detected by a Schmitt trigger, producing a squared pulse. Both edges are detected since this tends to subtract out errors due to noise. There is a sufficiently high correlation between the leading- and trailing-edge detection times such that the location of the signal-pulse center tends to be unaffected by the filtered noise. Therefore, the center of the squared logic pulse is assumed to be the center of the star image. A theoretical discussion of this is presented in the next section.

The output of the Schmitt trigger, in conjunction with the sweep frequency signal, controls logic gates which determine the direction of an up-down counter. These gates also provide a passage for the clock pulses going to the counter. The up-down counter operates in the up mode during time t_1 and in the down mode during time t_2. At the end of the complete counting period, the resulting digital number $(t_1 - t_2)$ is shifted to the output register for either display or recording purposes, or both.

THEORETICAL DISCUSSION

Signal-to-Noise Ratio

Since the basic noise mechanism is the same in a photomultiplier and an image dissector tube, the signal-to-noise ratio is calculated in the same manner. (See ref. 2.)

The noise in the signal is the only source being considered; other sources are negligible. The signal-to-noise ratio S/N is given by the following relation:

$$\frac{S}{N} = \frac{I_a}{(2e\mu I_a \, \Delta f \, k)^{1/2}} \tag{1}$$

where I_a is the signal current, e is the electron charge, μ is the current amplification, Δf is the noise bandwidth, and k is a statistical value due to electron multiplication.

Since time between signal pulses is being measured, the amplitude variations in the pulse determined by equation (1) must be converted to time variations. In order to make this conversion, the shape of the signal pulse must be known.

A circular star image has been used for all calculations and experiments in this report. The normalized pulse shape A for a circular image crossing a slit can be calculated from the following equation, since the signal current I_a is proportional to the area of the image that is seen by the transducer:

$$A = \frac{1}{\pi}\left[\cos^{-1}\left(1 - \frac{2t}{T_S}\right) - \left(1 - \frac{2t}{T_S}\right)\sqrt{\frac{4t}{T_S} - \left(\frac{2t}{T_S}\right)^2}\right] \qquad \left\{\begin{array}{l} 0 \leq t \leq T_S \\ 0 \leq \cos^{-1}\left(1 - \frac{2t}{T_S}\right) \leq \pi \end{array}\right\} \tag{2}$$

This equation is good for one edge of the signal pulse, the other edge being symmetrical. The equation will hold if the image diameter is equal to the slit width. The time t is any time between 0 and T_S, and T_S represents the time for the image to move from just outside of the slit to completely within the slit.

In figure 4, a nominal signal pulse and the predicted noise envelope (1σ) have been calculated by using equations (1) and (2). A nominal pulse is defined to be noise free. These calculations were made for a +11.5-magnitude star and a triangular sweep frequency of 50 hertz $(t_1 + t_2 = 0.02 \text{ sec})$. The middle curve is the nominal signal pulse normalized to a scale of 1. The slit width was selected to be the same size as the diameter of the star image, for maximum electrical signal. Therefore, an amplitude of 1 indicates that the image is completely within the slit of the transducer. However, because of the noise, the signal will vary from nominal. The upper and lower curves represent the calculated root-mean-square noise envelope for the 11.5-magnitude star. Notice that the largest amplitude variation is at the peak of the signal pulse where the signal-to-noise ratio is maximum. The signal-to-noise ratio decreases at the lower levels of the pulse. However, the actual noise amplitude has also decreased, since the nominal signal amplitude is getting smaller. It can be seen from the curve that the

actual time variation for any pulse is less at the lower threshold levels of the Schmitt trigger.

System-Stability Error

Statistical techniques can be used to determine the system-stability error. This technique is demonstrated by use of figure 5, which contains a nominal signal pulse, a typical signal pulse containing noise, and a logic pulse from the Schmitt trigger. These signals are referenced to an orthogonal coordinate system, the axes being amplitude and time.

The center of the nominal signal pulse, which is also the center of the star image, is located on the vertical axis. By definition, the center of the star image will have a value of zero time. The basic assumption used is that the measured signal-pulse center t_{mc} is always halfway between the leading-edge and trailing-edge detection times. Without noise the measured and actual signal-pulse centers will be identical. However, because of the noise described previously, there is a difference between the two. The error is defined as t_ϵ and can be calculated by

$$t_\epsilon = \frac{t_t - t_l}{2} = t_{mc} \tag{3}$$

The times t_l and t_t represent the times from the center of the signal pulse to the leading and trailing edges, respectively. If the time periods t_l and t_t are equal, then $t_\epsilon = t_{mc} = 0$.

The standard deviation σ_n for both the leading- and trailing-edge times is (ref. 3):

$$\sigma_n = \sqrt{\frac{\sum_{n=1}^{K} (\delta t_n)^2}{K - 1}} \tag{4}$$

where n represents the sample number and K is the number of samples.

The deviation from the arithmetic average δt_n can be found by

$$\delta t_n = t_n - \bar{t} \tag{5}$$

and the arithmetic average time $\bar{t}$ is

$$\bar{t} = \frac{\sum_{n=1}^{K} t_n}{K} \tag{6}$$

As mentioned previously, there is a high correlation between the leading- and trailing-edge detection times. The actual correlation coefficient ρ can be found by

$$\rho = \frac{1}{(K - 1)\sigma t_l \sigma t_t} \sum_{n=1}^{K} \left(\delta t_{ln} \delta t_{tn}\right) \tag{7}$$

The standard deviation for the time error in the measured signal-pulse center σt_ϵ is calculated for the definition of t_ϵ given in equation (3), as follows:

$$\sigma t_\epsilon = \sqrt{\left(\frac{\partial t_\epsilon}{\partial t_l}\right)^2 \sigma t_l{}^2 + \left(\frac{\partial t_\epsilon}{\partial t_t}\right)^2 \sigma t_t{}^2 + 2\rho\left(\frac{\partial t_\epsilon}{\partial t_l}\right)\left(\frac{\partial t_\epsilon}{\partial t_t}\right)\sigma t_l \sigma t_t} \tag{8}$$

Equations (4) to (8) can be found in reference 3.

It can be seen that if the correlation coefficient is unity (perfect correlation), the standard deviation will reduce to

$$\sigma t_\epsilon = \frac{1}{2}\left(\sigma t_t - \sigma t_l\right)$$

since

$$-\frac{\partial t_\epsilon}{\partial t_l} = +\frac{\partial t_\epsilon}{\partial t_t} = \frac{1}{2}$$

Therefore, if the standard deviation for both the leading and trailing signal edges are equal and remain equal for any threshold level, the detected pulse center will have zero variation for $\rho = 1$.

Data-Averaging Effects

The next step is to calculate the total system-stability error E for a complete cycle. Refer to the pulse train in figure 2 and let t_{ϵ_1}, t_{ϵ_2}, and t_{ϵ_3} represent the error

between the measured and actual signal-pulse centers for the first, second, and third pulses, respectively.

There are two basic measurements – one for the up count and one for the down count:

$$\text{Up count} = t_1 \pm t_{\epsilon_1} \pm t_{\epsilon_2}$$

$$\text{Down count} = t_2 \pm t_{\epsilon_2} \pm t_{\epsilon_3}$$

Both measurements are dependent upon t_{ϵ_2}. If this error is in a direction to increase t_1, then t_2 will be smaller by the same amount. Therefore, t_{ϵ_2} will be weighted twice in the final system computation.

The output number N can be computed as follows:

$$N = t_1 - t_2 \pm t_{\epsilon_1} \pm 2t_{\epsilon_2} \pm t_{\epsilon_3} \tag{9}$$

The system-stability error E can be calculated by the same method as equation (8) with $\rho = 0$:

$$E = \sigma N = \pm\sqrt{\left(\sigma t_{\epsilon_1}\right)^2 + 4\left(\sigma t_{\epsilon_2}\right)^2 + \left(\sigma t_{\epsilon_3}\right)^2}$$

If $\sigma t_\epsilon = \sigma t_{\epsilon_1} = \sigma t_{\epsilon_2} = \sigma t_{\epsilon_3}$,

$$E = \pm\sqrt{6}\,\sigma t_\epsilon \tag{10}$$

When signal pulses of two or more measuring periods are averaged, all of them will have a weighting of 2 except the first and last pulses. The formula can be extended for an average of P measurements, as follows:

$$E = \pm\frac{1}{P}\sqrt{\left(\sigma t_{\epsilon_1}\right)^2 + 4\left\{\left(\sigma t_{\epsilon_2}\right)^2 + \ldots + \left[\sigma t_{\epsilon_{(p-1)}}\right]^2\right\} + \left(\sigma t_{\epsilon_p}\right)^2}$$

where $p = 2P + 1$ and p represents the pulse number. For $\sigma t_\epsilon = \sigma t_{\epsilon_1} = \ldots = \sigma t_{\epsilon_p}$,

$$E = \pm\frac{\sqrt{2(4P - 1)}}{P}\,\sigma t_\epsilon \tag{11}$$

As P increases, the system-stability error will become inversely proportional to the square root of P. For $P = 1$, equation (11) reduces to equation (10).

Derivation of System-Stability Error as a Function of Star Magnitude

If the system-stability error is known for one star magnitude m_1, then it can be determined for any other star magnitude m_2 as follows:

From the stellar magnitude equation,

$$m_1 - m_2 = 2.51 \log F_r$$

or

$$F_r = 10^{\left(\frac{m_1 - m_2}{2.51}\right)}$$

where F_r is the ratio of light intensity for stars 2 and 1, respectively.

The transducer output I_a varies directly with the incoming light intensity F, namely,

$$I_a \propto F$$

From equation (1) it has been shown that the square of the signal-to-noise ratio varies directly with the signal current – that is,

$$\left(\frac{S}{N}\right)^2 \propto I_a$$

and causes the noise envelope in figure 4 to vary.

The standard deviation for both the leading- and trailing-edge times decreases as the signal-to-noise ratio increases

$$\sigma t_l \propto \left(\frac{S}{N}\right)^{-1}$$

$$\sigma t_t \propto \left(\frac{S}{N}\right)^{-1}$$

This relationship is maintained for threshold levels of interest (30 to 70 percent). Beyond these limits, nonlinearities become evident.

According to equations (7) and (8), the standard deviation in the measured signal-pulse center varies directly with the standard deviation of each edge. This type of variation assumes a symmetrical pulse, as follows:

$$\sigma t_\epsilon \propto \sigma t_l \propto \sigma t_t$$

Equation (11) shows that the system-stability error varies directly as the time variation in the measured signal-pulse center, or

$$E \propto \sigma t_\epsilon$$

From the proportionalities given, it has been shown that the system-stability error varies inversely with the signal-to-noise ratio:

$$E \propto \left(\frac{S}{N}\right)^{-1}$$

Therefore,

$$E_r = 10^{\left(\frac{m_1 - m_2}{5.02}\right)} \tag{12}$$

where E_r is the ratio of system-stability error for stars 1 and 2.

TRANSDUCER EXPERIMENTS AND RESULTS

General

Experiments have been conducted with an image dissector tube, the operation of which is discussed previously in the section entitled "Description of Star Sensor." This transducer is extremely flexible. The sweep frequency, amplitude, and type of sweep (i.e., triangular, sinusoidal, or other) may be changed very easily. The sweep amplitude was kept constant at ±28 image diameters (-0, +7 percent) for all testing. This amplitude is equivalent to a field of view of ±2 arc seconds for the 3-meter f/100 telescope configuration.

The experiments reported herein have been made for a single-axis system. However, both the theory and experimental data are applicable to a two-axis system. The sweep signal and defining aperture would change, but the basic approach would remain the same.

In the sections that follow, the experimental apparatus is first described, and the results of experiments to determine system errors are then presented. The system errors are discussed in terms of image diameters which relate directly to angular errors (0.01 arc sec = 0.14 image diameters). The total variation as given in terms of two standard deviations ($\pm 2\sigma$). Approximately 75 samples are used for all the experiments. Furthermore, all magnitudes given are referenced to an AO$\underline{\overline{V}}$ star at a color temperature of 10 700^{O} K. In addition, a 10.9-percent reduction in intensity is used to account for central obscuration. Further discussion of star-magnitude calibration is presented in appendix A and reference 4.

Experimental Apparatus

The laboratory configuration consists of a source which simulates the star, a collecting lens, an image dissector, and digital electronics which process the transducer signals. A schematic of the laboratory configuration is shown in figure 6. The oscilloscope and camera are used to obtain time histories of star crossings.

The optical system is chosen to project an image of a circular aperture onto the focal plane of a simulated diffraction-limited, 3-meter f/100 telescope; the diameter of the image is equal to the diameter of the first dark ring of the airy disk. For convenience of testing, the angular motion per linear displacement of the image on the focal plane was increased by a factor of 1000 over that for an f/100 telescope. Parameters for this laboratory experiment are shown in table I.

TABLE I.- OPTICAL PARAMETERS

Focal length of lens	26.7 cm
Source diameter	762 μm
Image diameter	106.7 μm
Image distance	30.5 cm
Object distance	218 cm
Lens diameter	3.81 cm
Scale factor	1000

A photograph of the physical layout of a part of this system is shown in figure 7. The lens is contained in the vertical holder at the right. The image dissector is located in the cylindrical tube and is mounted on a movable, two-axis calibrated base. The front face of the image dissector is located at the focal plane just behind a shutter. Some of the electronics can be seen mounted on the rear of the base.

Variation of Frequency

A parametric study relating system stability, sweep frequency, and star magnitude was made. A triangular sweep at frequencies of 12.5, 25, 50, 100, and 200 hertz was used. A plot of the system error as a function of star magnitude for these frequencies is shown in figure 8. A 12.4-magnitude star is the dimmest source that can be observed at a frequency of 12.5 hertz. At a frequency of 100 hertz, an 11.1-magnitude star can be seen; at a frequency of 200 hertz, a 10.7-magnitude star can be seen. The logarithm of the system stability is shown to be proportional to the star magnitude. As expected, the system stability decreases as the star magnitude increases, for any sweep frequency. Also, the system stability decreases as the frequency increases. It should be noted that the noise filter bandpass Δf was changed in direct relationship with the sweep frequency. A bandpass of 5.8 kilohertz was used for a sweep frequency of 100 hertz. From the 12.5-hertz curve, the data indicate that a change of 5 star magnitudes will cause the system error to change by a factor of 10. These results agree with equation (12).

The curves in figure 8 have been drawn parallel to each other and spaced in proportion to the square root of the frequency, as evidenced by equations (1) and (2). Although the data points seem to be spread out for the brightest stars, they are within the counting resolution for the system. The basic counting rate of 160 kilohertz is the same for all sweep frequencies. Therefore, as the sweep frequency increases, each clock pulse represents a greater distance on the focal plane. For example, at a sweep frequency of 12.5 hertz, the clock pulse can divide the image into 16 times the number of parts that would be obtained at a frequency of 200 hertz. The resolution of one counting pulse for each sweep frequency is shown in table II.

TABLE II.- SWEEP FREQUENCY RESOLUTION

Frequency, Hz	Resolution, image diameters
12.5	0.00223
25	.00446
50	.00893
100	.0178
200	.0357

The basic system clock-pulse error for any measurement is ±2 pulses, which is due to separate forward and backward time measurements. Since this count variation is independent of star magnitude, it represents a large percentage of the total error for the brightest stars. For this reason, all the data points for the brighter stars have errors that are greater than that shown by the curves of figure 8. For stars of higher magnitude,

the count variation becomes masked, and hence the errors in the data points are both above and below the curves.

Variation of Threshold

Two separate tests were made to determine how the system stability varies with the threshold level. Threshold level is defined as the level at which the signal pulse is detected. (See fig. 3.) The results are shown in figures 9 and 10.

In the first test (fig. 9), a triangular sweep frequency of 12.5 hertz was used, and the threshold level was varied from 10 to 70 percent of the nominal pulse amplitude. In the second test (fig. 10), a sweep frequency of 100 hertz was used; however, the data were averaged over two cycles, yielding a simulated frequency of 50 hertz. It will be shown in the next section that this simulation was valid. In this test the threshold was varied from 20 to 80 percent of the nominal amplitude. In both cases the threshold level has little effect on system stability. However, to minimize stray noise pulses at low threshold levels and the possibility of missing signal pulses at high threshold levels, the best operating level was found to be 30 to 50 percent.

The larger variations in figure 10 are caused by the low resolution of the counting pulse. This value is 1/4 of the sweep frequency of 12.5 hertz. The data compare well with the results of the 50- and 12.5-hertz curves in figure 8. In figure 9 the dashed lines indicate that a poor experimental data point has been omitted.

Four photographs containing a squared logic pulse and signal pulse out of the bandpass filter are shown in figure 11. They are for an 11.5-magnitude star at a sweep frequency of 50 hertz. The center of the star image is at the peak signal-pulse amplitude. It can be seen that both the times t_t and t_l tend to increase or decrease for any given pulse. Since the time variations tend to subtract, threshold level has little effect. These photographs also establish the validity of the assumptions previously made in the analysis.

It is preferable to measure t_l and t_t with respect to a reference pulse generated by the synchronization signal. The reference signal always occurs at the same time with respect to the center of the star image. This method eliminates the uncertainty involved in determining the center of the time axis in figure 5.

Data Averaging

A test was made to observe the effect of averaging on system stability. A sine wave frequency of 100 hertz was used as the basic reference frequency. Data were first taken for every cycle, and then averages over 2, 4, and 8 cycles were used.

In figure 12 the system-stability error is presented as a function of star magnitude for the number of cycles averaged. All data points are within the basic system counting

accuracy except those for a 10.5-magnitude star at averages of 2, 4, and 8. A possible explanation is that the guide star simulator was brighter than that measured.

As expected, the stability improves as the number of pulses averaged increases, the error being proportional to the square root of the system average. For the measurements taken, the system average is equivalent to the frequencies listed in table III:

TABLE III.- EQUIVALENT FREQUENCIES DUE TO AVERAGING

Average	Equivalent frequency, Hz
1	100
2	50
4	25
8	12.5

From these data and from the theory presented, the system-stability error can be determined for any combination of sweep wave form, sweep frequency, system average, and star magnitude.

Linearity and Field of View

A test was made to record the measured output number as a function of image displacement, using a triangular sweep. The transducer, which was mounted on a calibrated micrometer base, was physically moved so as to simulate the effect of image displacement. A digital output number was recorded for each position of the transducer.

A graph plotting the percentage deviation from the best straight line as a function of image displacement is shown in figure 13. The system is shown to be linear within ±0.6 percent of best straight line over the entire range. Since the electrical source used to supply the reference sweep signal has a specification of 1 percent over the entire range, the transducer may have much better linearity than shown. The total field of view is 60 image diameters (6.35 mm), which is a large dynamic range for this type of sensor.

A design technique was included in the digital electronics to get maximum use of the total field of view. Assume that the dotted line in figure 2 representing star-image position approaches the maximum extreme of the triangular sweep. Two of the three output pulses will approach each other. At some finite position near the end of the sweep, the two signal pulses become one pulse. The digital electronics detects this condition and divides them into two squared pulses with a preset time interval as shown in figure 14.

Trace A in figure 14 is the sync pulse which represents a change in sweep direction. Trace B is the signal pulse, and traces C and D are logic pulses. The first three

photographs (parts (a), (b), and (c)) show two distinct signal pulses. In figure 14(d), the pulses have essentially collided. The digital logic has separated the one squared pulse D into two parts. This separation is shown by the two breaks, which are flagged, of 4-μsec duration each on trace C. The field could have been extended further had the sync pulse A been delayed by 130 μsec to compensate for the phase shift of the signal pulses caused by the signal conditioning electronics.

CONCLUSIONS

An investigation has been made to design and test a fine-pointing star sensor that could detect star-image motion on the focal plane of a telescope and generate position information. This result was successfully accomplished. The measuring technique employed has proven to be very practical. Pulses from the image dissector are inherently digital and with a little signal conditioning (amplification, filtering, and squaring) can be ready for digital processing. The versatility of the image dissector allows great flexibility to the user. The sweep frequency, amplitude, and the type of sweep (triangular, sinusoidal, or other) can be easily changed.

Experimental results show that the transducer is capable of measuring stars within the accuracy desired. When guiding on a +10-magnitude star, the system-stability error is 0.08 image diameter for a triangular sweep frequency of 100 hertz. The system-stability error has been measured for several different star magnitudes and sweep frequencies. The results have shown that if the stability is known for one star magnitude and sweep frequency, then it can be determined for any other magnitude and frequency. Both the data and theory have shown that the logarithm of the system-stability error is proportional to the star magnitude. Other test results have shown that the system-stability error improves as the number of counting periods averaged increases, the error being inversely proportional to the square root of the number of counting periods. This result was also predicted in the theoretical section.

When the signal pulses are detected on both the leading and trailing edges, the effect of threshold level becomes negligible. This effect is not negligible for single-edge detection. Furthermore, the time variations for both edges tend to subtract out. The system has been shown to be linear within 0.6 percent of best straight line over the complete range of 60 image diameters, which is a large dynamic range for this type of sensor.

Langley Research Center,
National Aeronautics and Space Administration,
Langley Station, Hampton, Va., March 25, 1969,
125-19-03-12-23.

APPENDIX A

CALCULATION OF STAR MAGNITUDE

In the laboratory experiments a small aperture (3.81 cm) is used to collect light from the star simulator. Since this configuration must simulate the effect of a 3-meter-diameter Cassegrain telescope, a scale factor must take into account the different collecting areas. This scale factor is proportional to the ratio of the areas, as shown by the following equation:

$$R = \frac{A_t}{A_l} = \frac{A_p - A_s}{A_l} \tag{A1}$$

For the transducer to see an equivalent star magnitude, a much brighter star must be used for the simulation. The increased star magnitude Δm can be calculated as follows:

$$\Delta m = \frac{\log R}{\log 2.51} \tag{A2}$$

For a scale factor of 5700 the star simulator should be 9.4 magnitudes brighter than a star viewed by a 3-meter telescope. The transducer will see the same star brightness for either case.

A reference must be used for any discussion of star magnitude. In the present study, all star magnitudes are referenced to an $AO\overline{V}$ star at a color temperature of 10 700° K when seen by the S-20 transducer used in the experiment.

The method used to measure star intensity is similar to that used on the OAO (Orbiting Astronomical Observatory) project. The calibration method (ref. 4) includes a star simulator for which the absolute spectral irradiance produced at the objective of the receiver being evaluated is known. The equivalent star magnitude of the simulator as seen by the transducer can be calculated by the following equation for stellar magnitude:

$$m = 2.51 \log \frac{\int H_{AO\overline{V}} R_\lambda \, d\lambda}{\int H_{SS} R_\lambda \, d\lambda} \tag{A3}$$

During the experiment calibration, the transducer signal current was measured, as the distance between the star simulator and collecting aperture was varied. Several data points were measured with the use of two different light sources in the star simulator.

APPENDIX A

These data are plotted in figure 15 and show that the logarithm of the signal current is a linear function of star magnitude. The increased star magnitude Δm of 9.4 has been taken into account in this figure.

Once the relationship between star magnitude and signal current is known, any source can be used to simulate the star. The measured signal current can be related to an equivalent star magnitude by using the calibration curve.

REFERENCES

1. Anon.: A System Study of a Manned Orbiting Telescope. D2-84042-1 (Contract NAS 1-3968), Boeing Co., Oct. 1965.

2. Eberhardt, E. H.: Signal-to-Noise Ratio in Image Dissectors. Res. Memo. No. 386, ITT Ind. Labs., July 1964.

3. Beers, Yardley: Introduction to the Theory of Error. Second ed., Addison-Wesley Pub. Co., Inc., 1962.

4. Draper, Lawrence T.: Star Tracker Calibration. NASA TN D-4594, 1968.

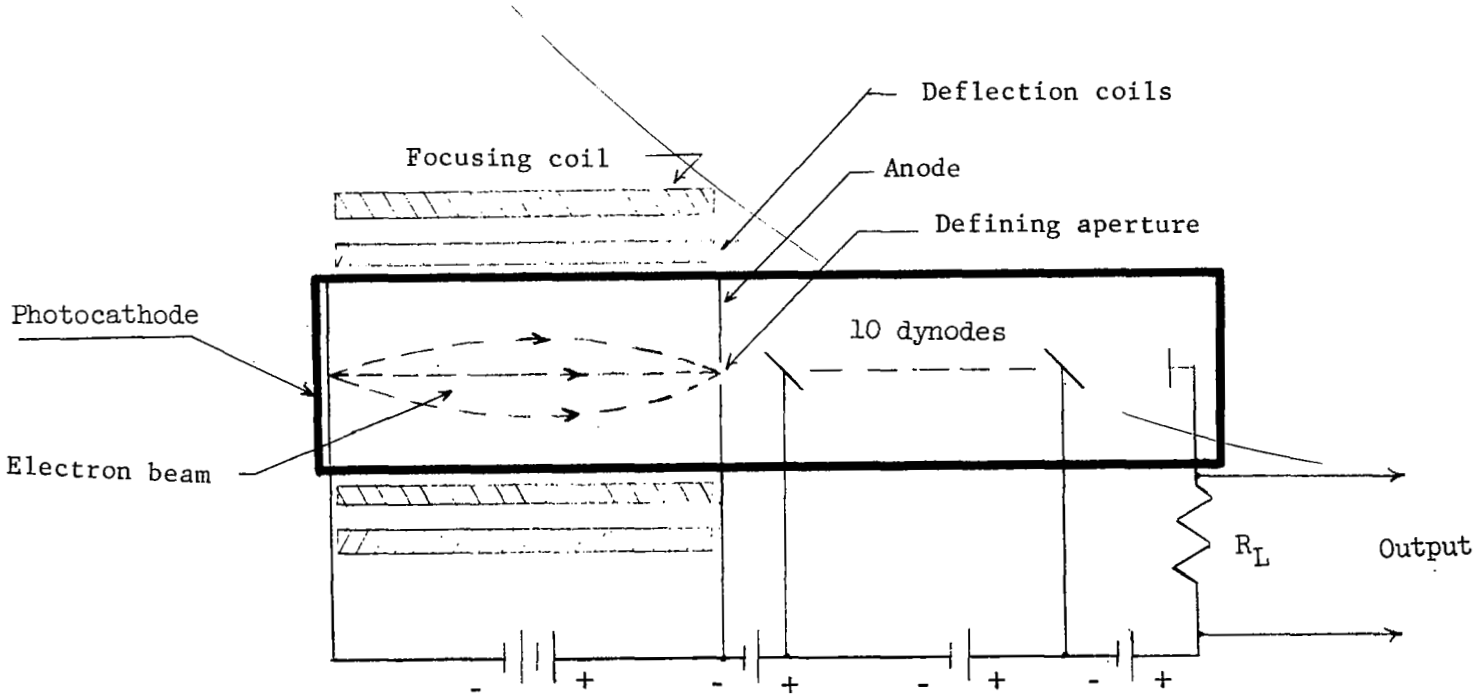

Figure 1.- Schematic representation of image dissector.

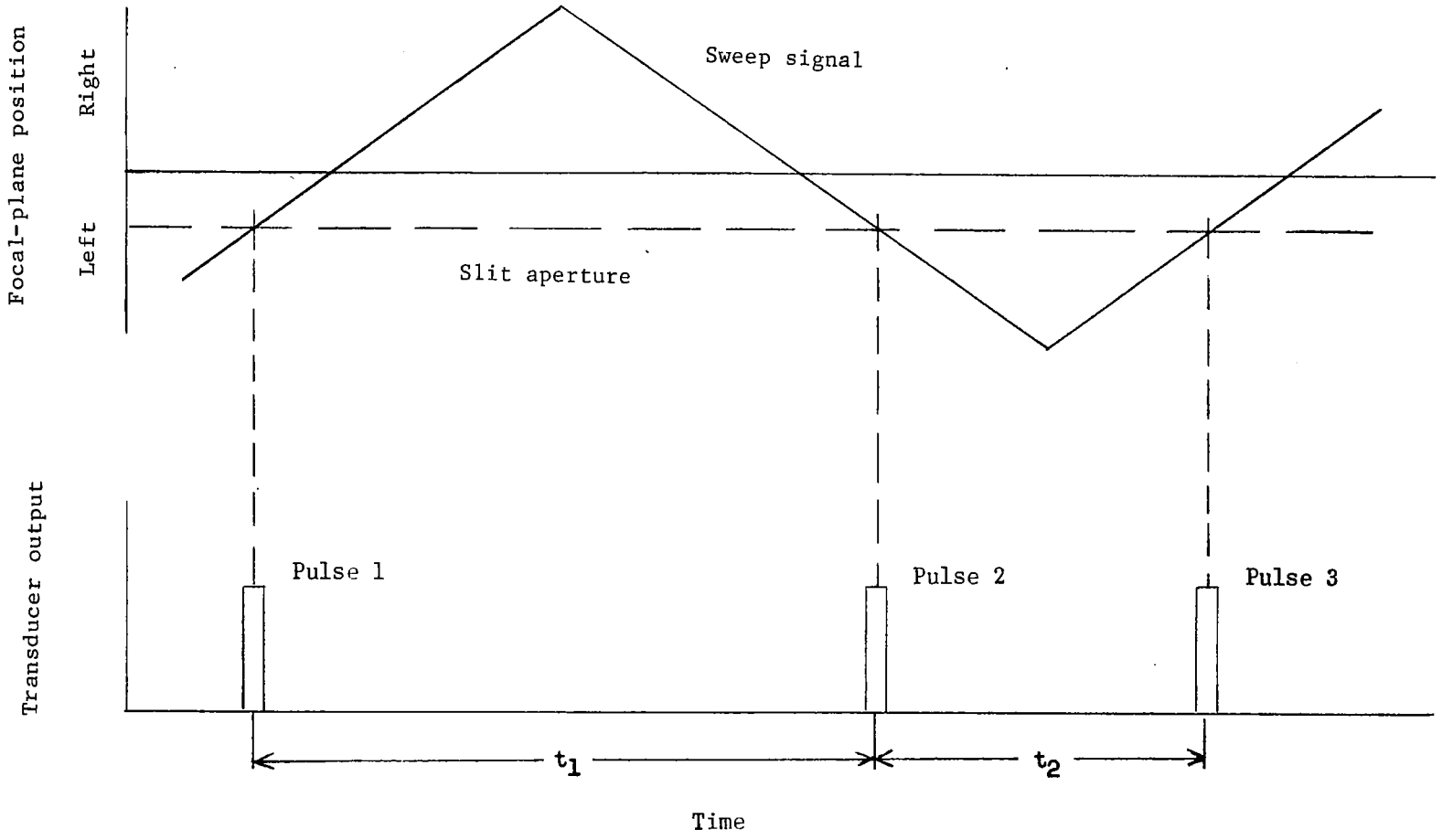

Figure 2.- Schematic representation of typical sweep signal and output pulses.

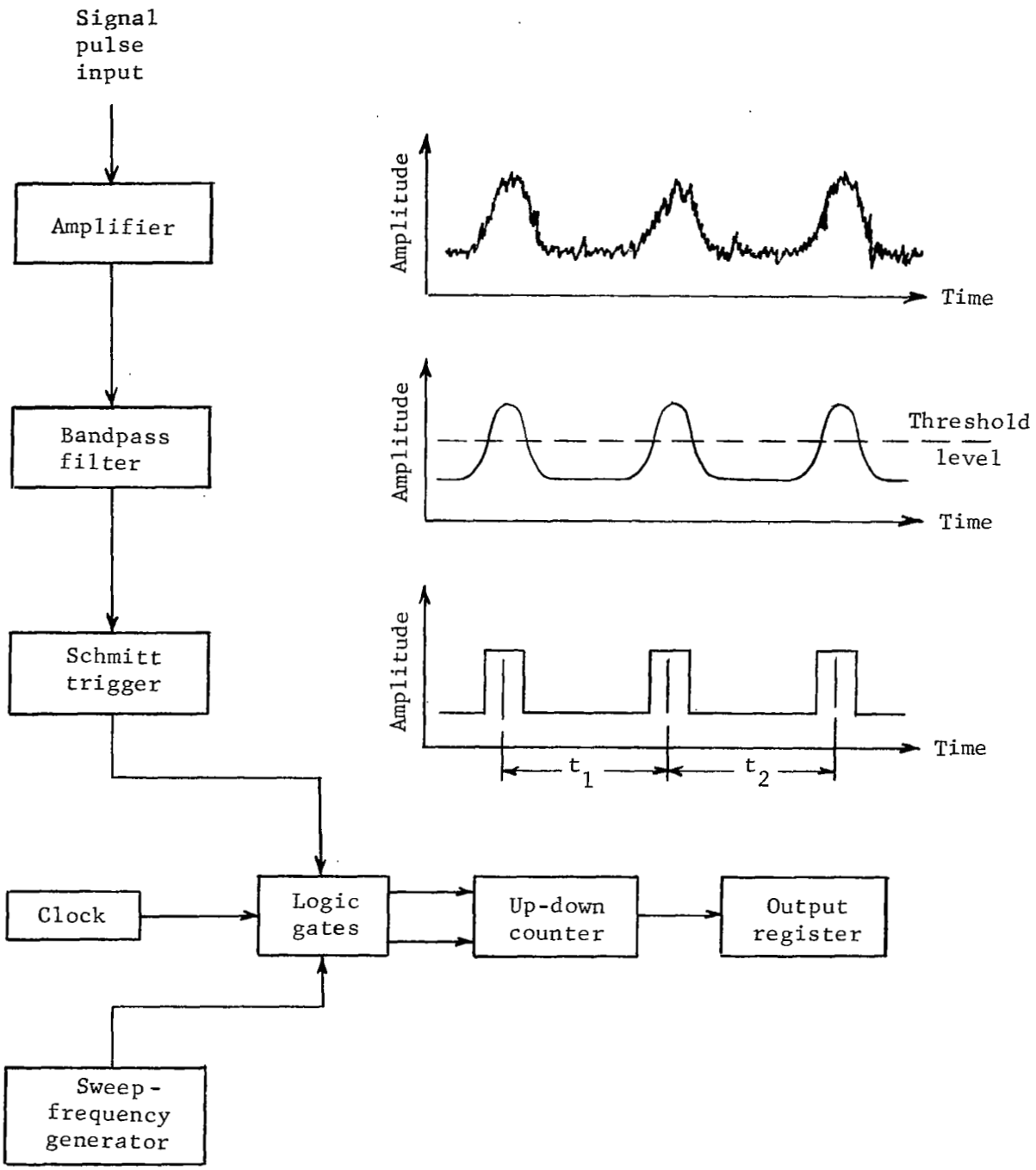

Figure 3.- Schematic representation and typical waveforms of signal-processing system.

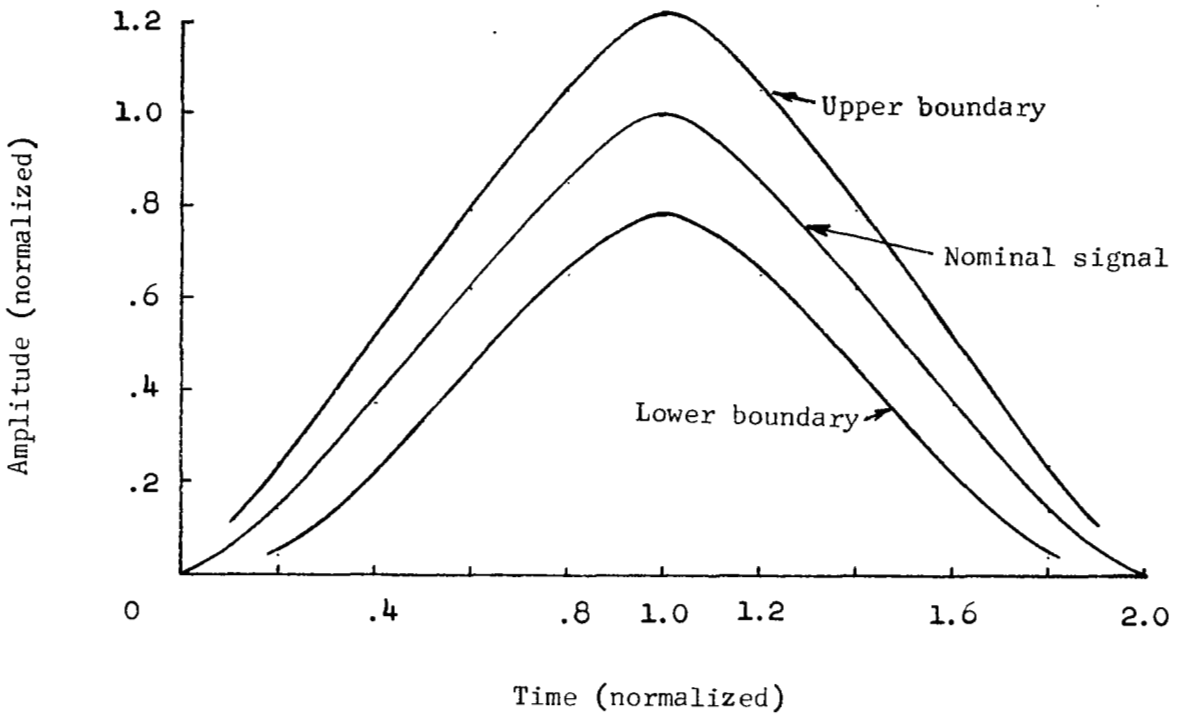

Figure 4.- Typical signal pulse with noise envelope.

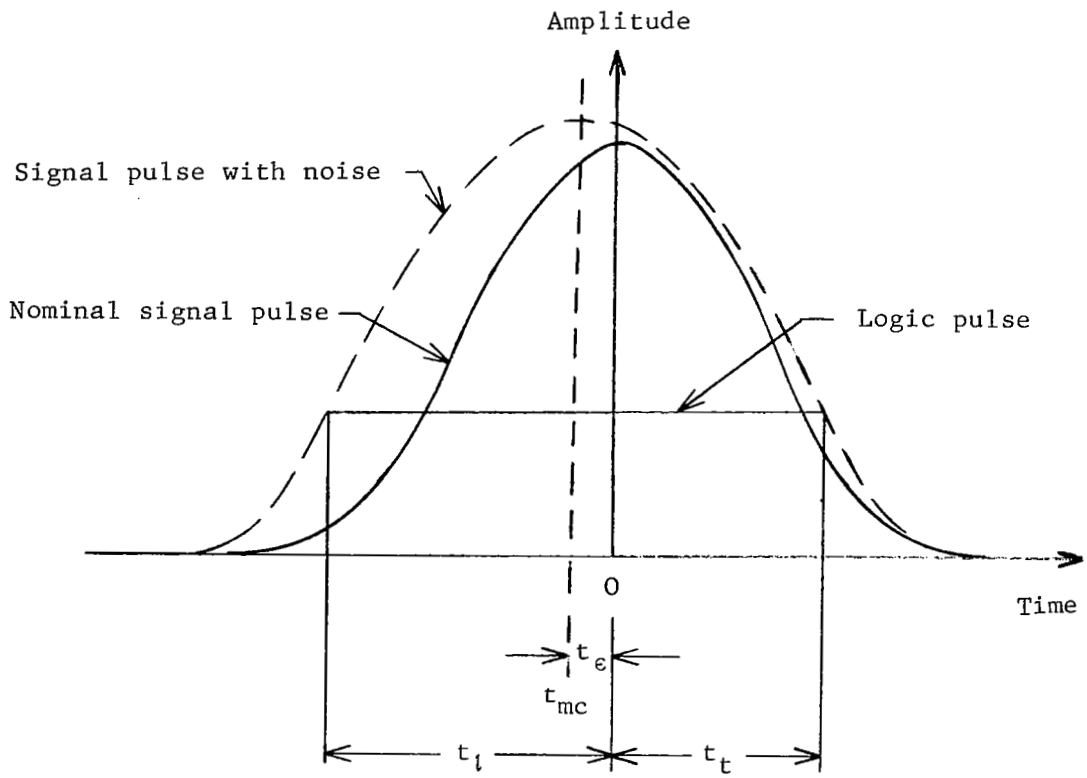

Figure 5.- Idealized signal pulse, typical signal pulse containing noise, and logic pulse from Schmitt trigger.

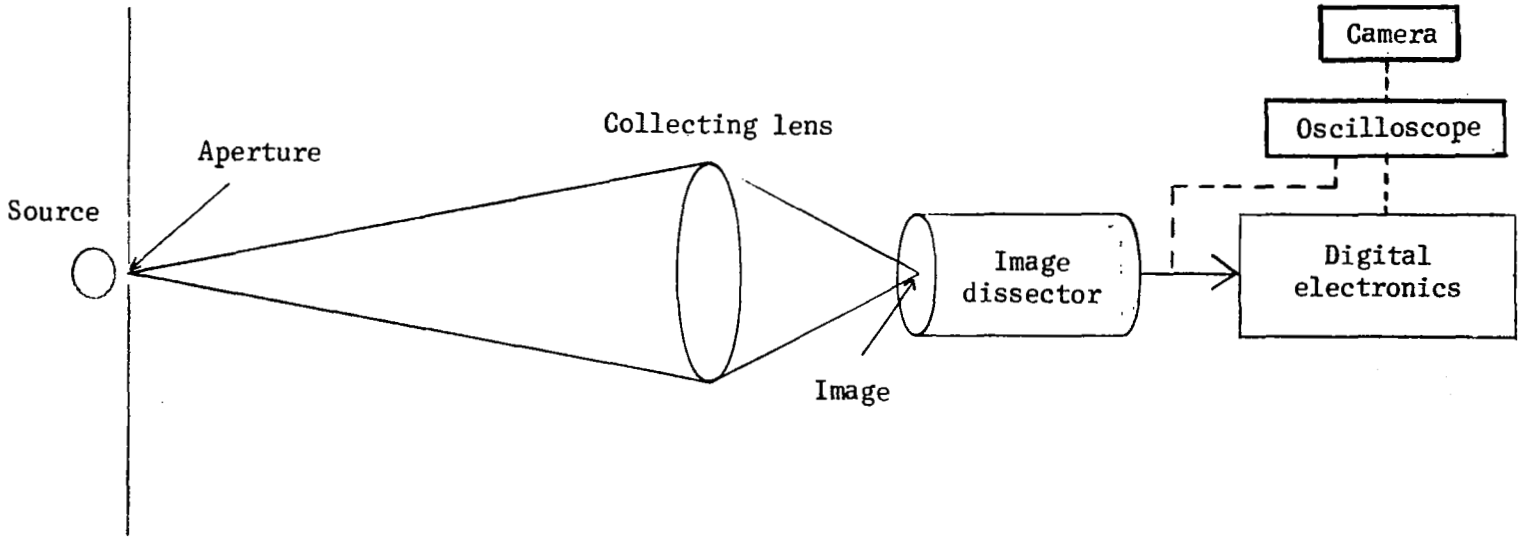

Figure 6.- Schematic of laboratory configuration.

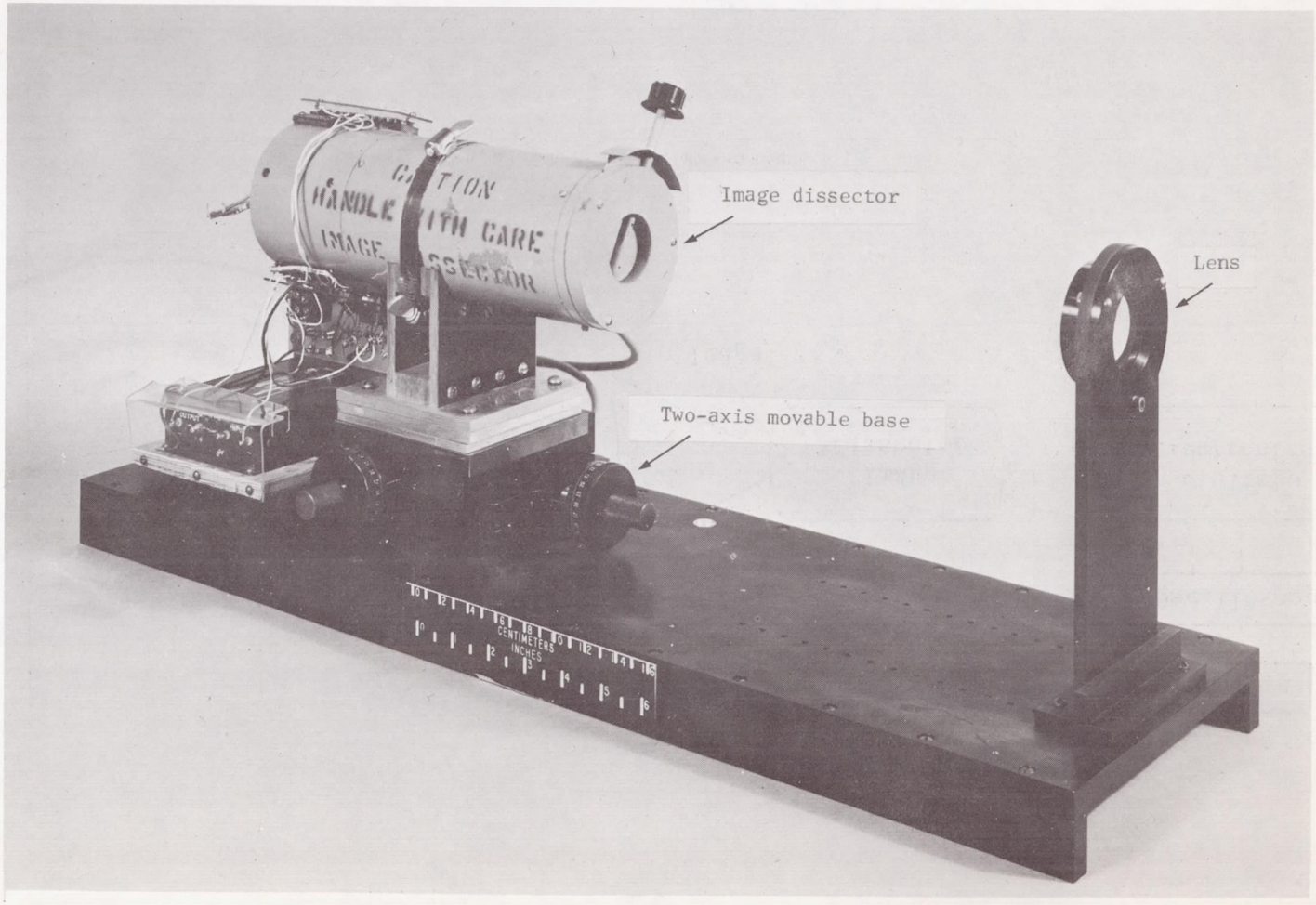

Figure 7.- Laboratory test model showing micrometer base, image dissector, and lens.

L-67-6133

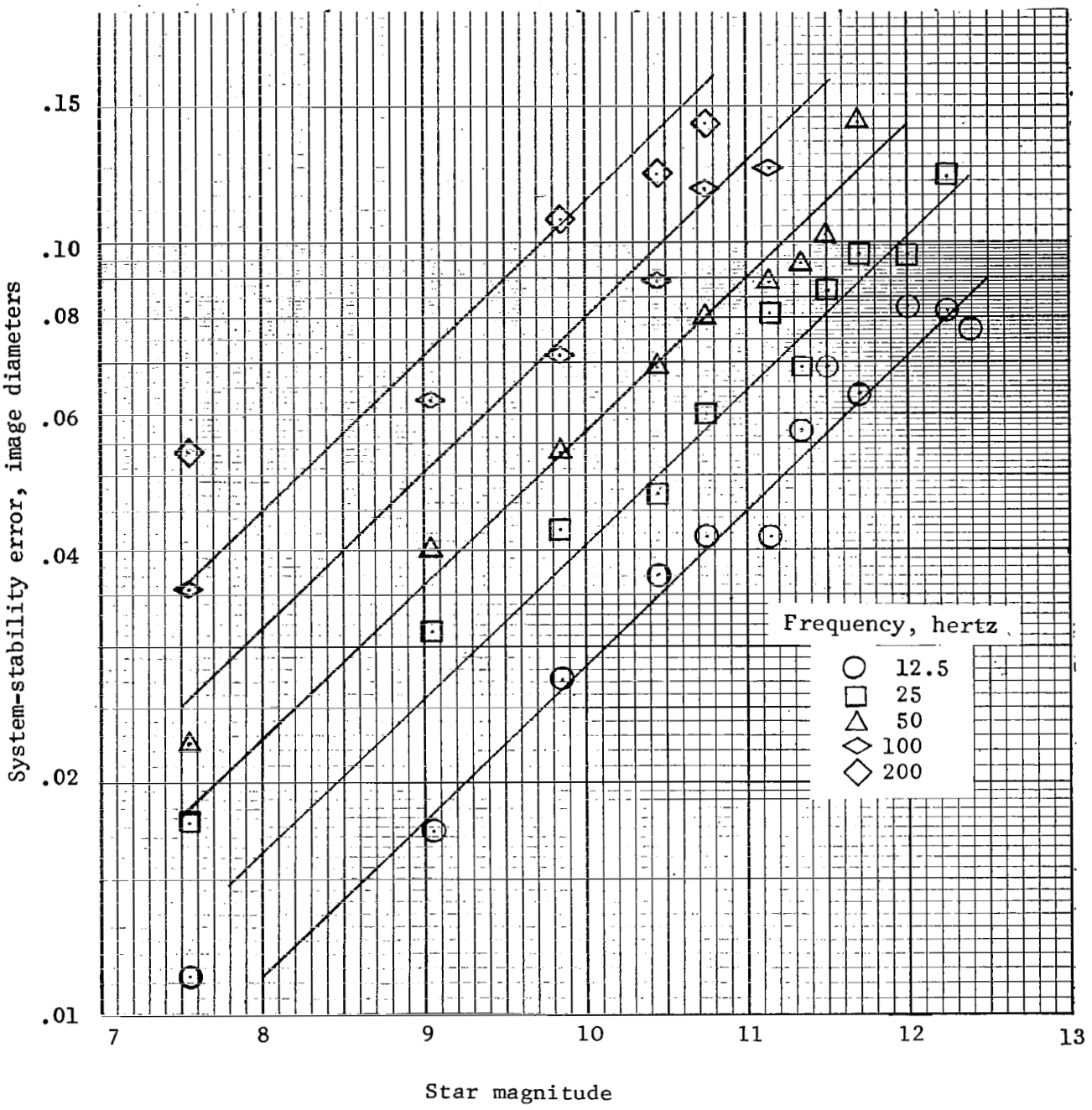

Figure 8.- Variation of system-stability error with star magnitude for several sweep frequencies.

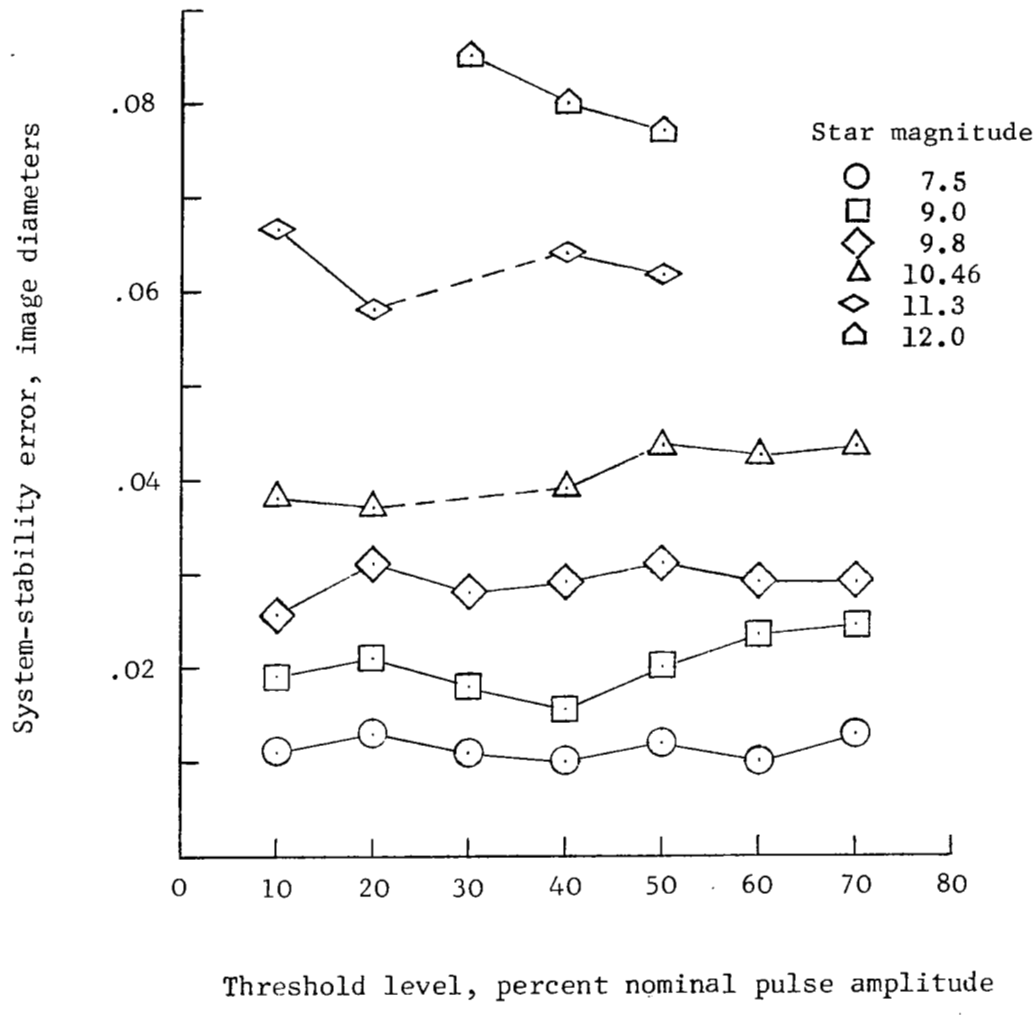

Figure 9.- Change in system-stability error as a function of threshold level for several star magnitudes and triangular sweep frequency of 12.5 hertz.

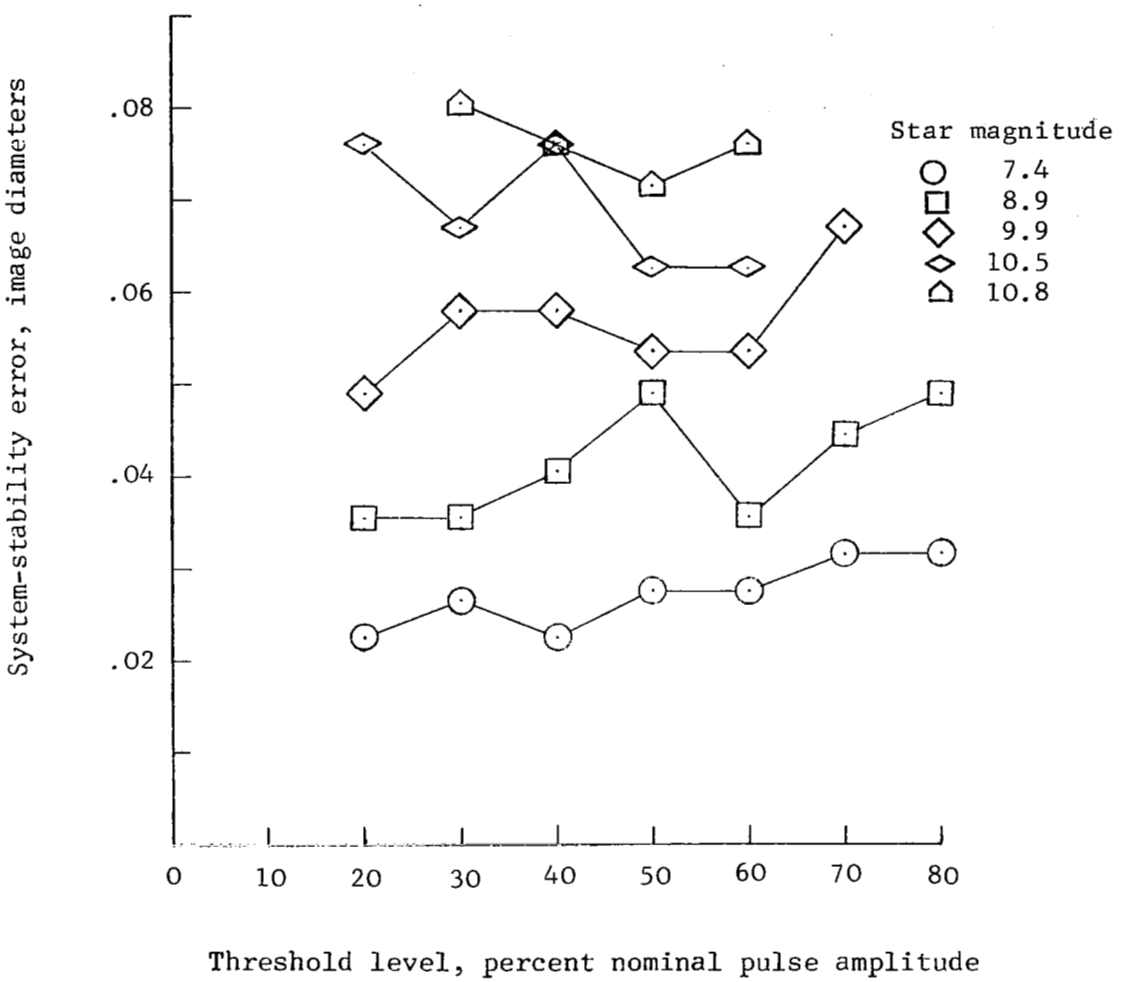

Figure 10.- Change in system-stability error as a function of threshold level for several star magnitudes and triangular sweep frequency of 100 hertz.

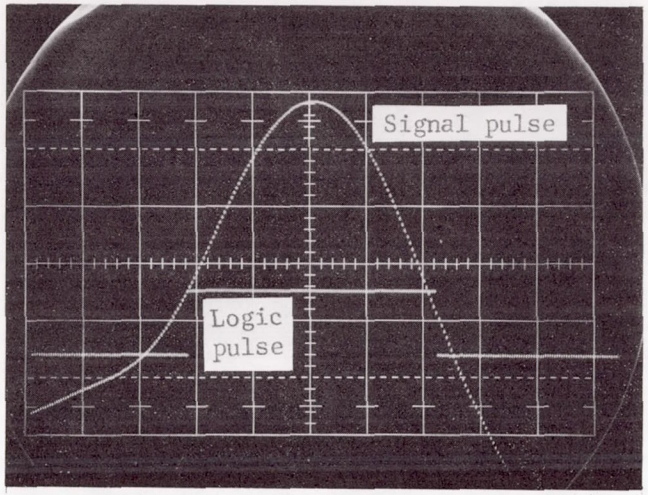

(a)

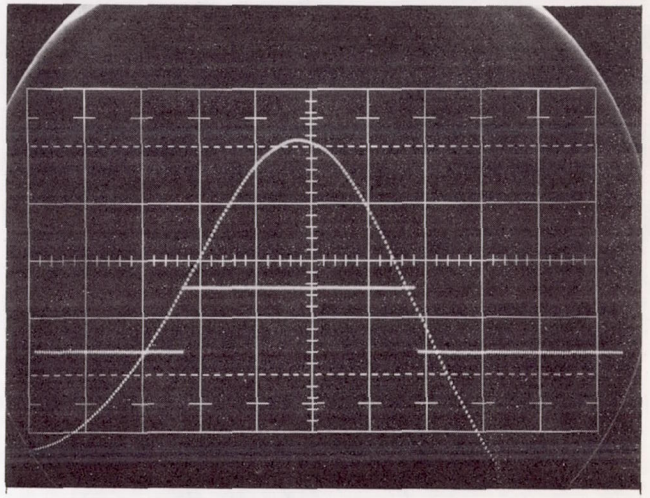

(b)

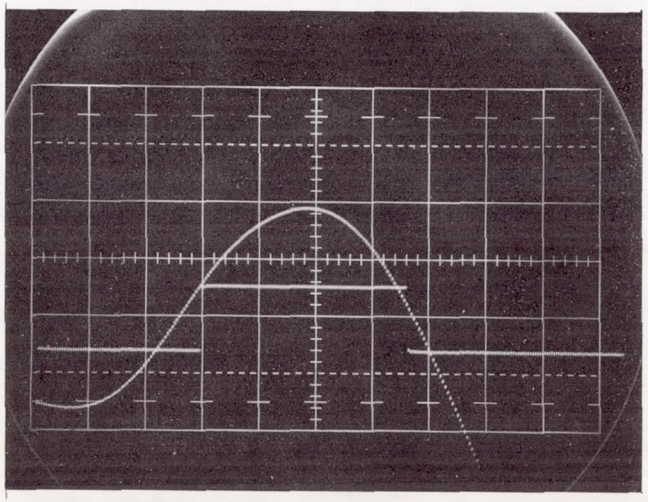

(c)

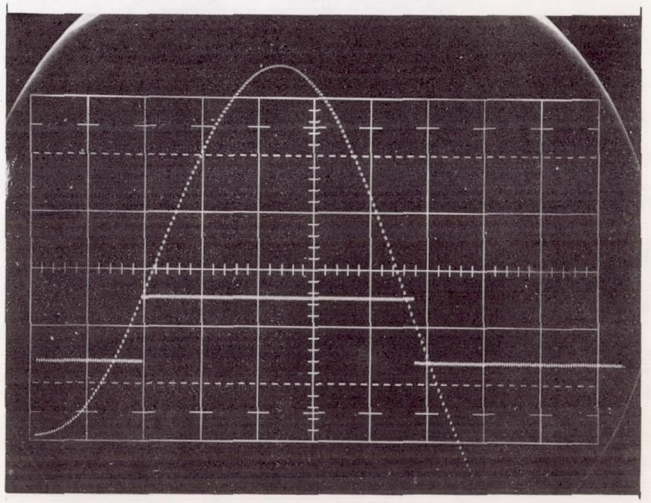

(d)

Figure 11.- Photographs of image-dissector pulse showing variation in signal pulse due to noise after filtering. Star magnitude, 11.5; sweep frequency, 50 hertz.

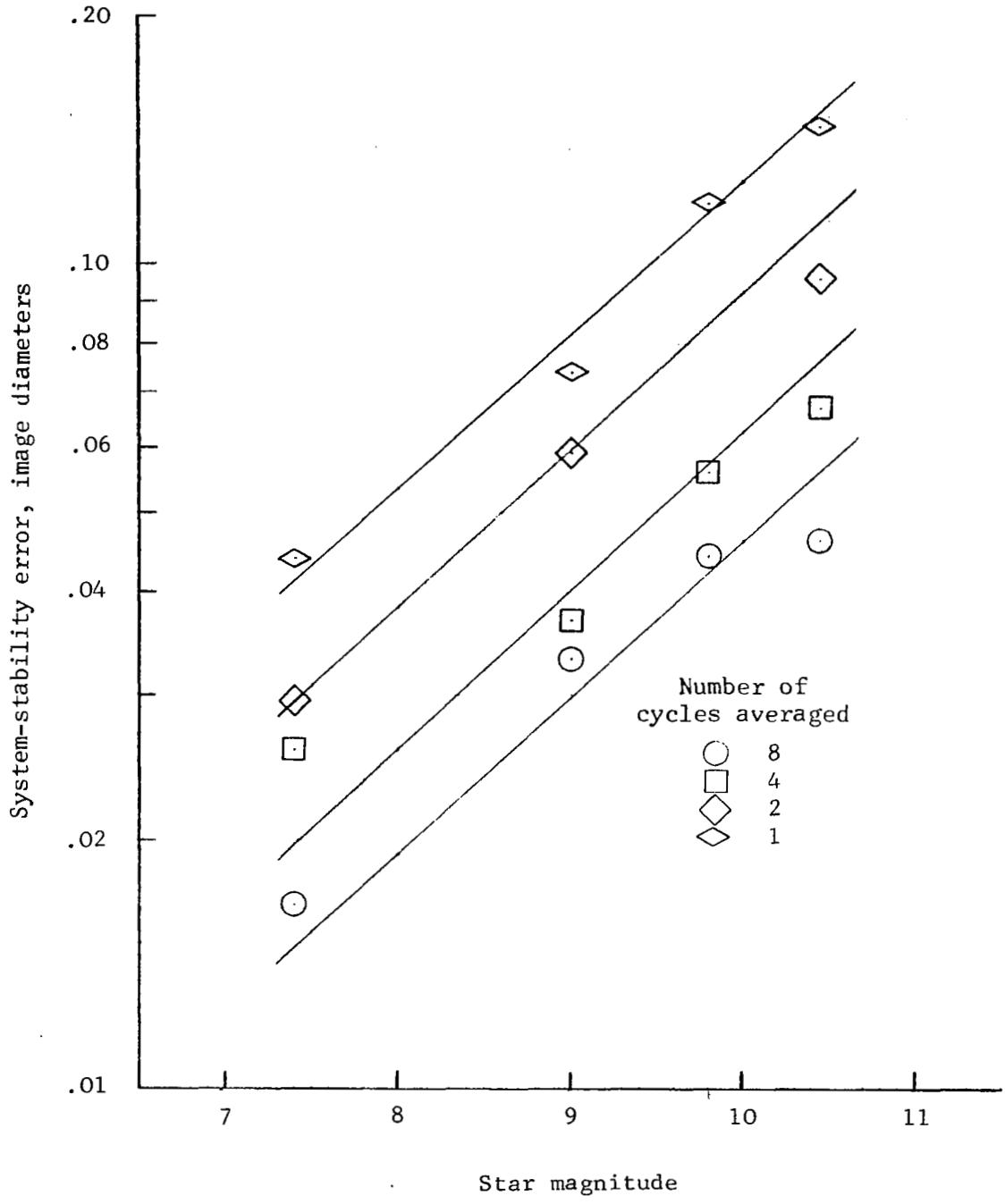

Figure 12.- Variation of system-stability error with star magnitude for data averaged over 1, 2, 4, and 8 cycles. Sweep frequency, 100 hertz.

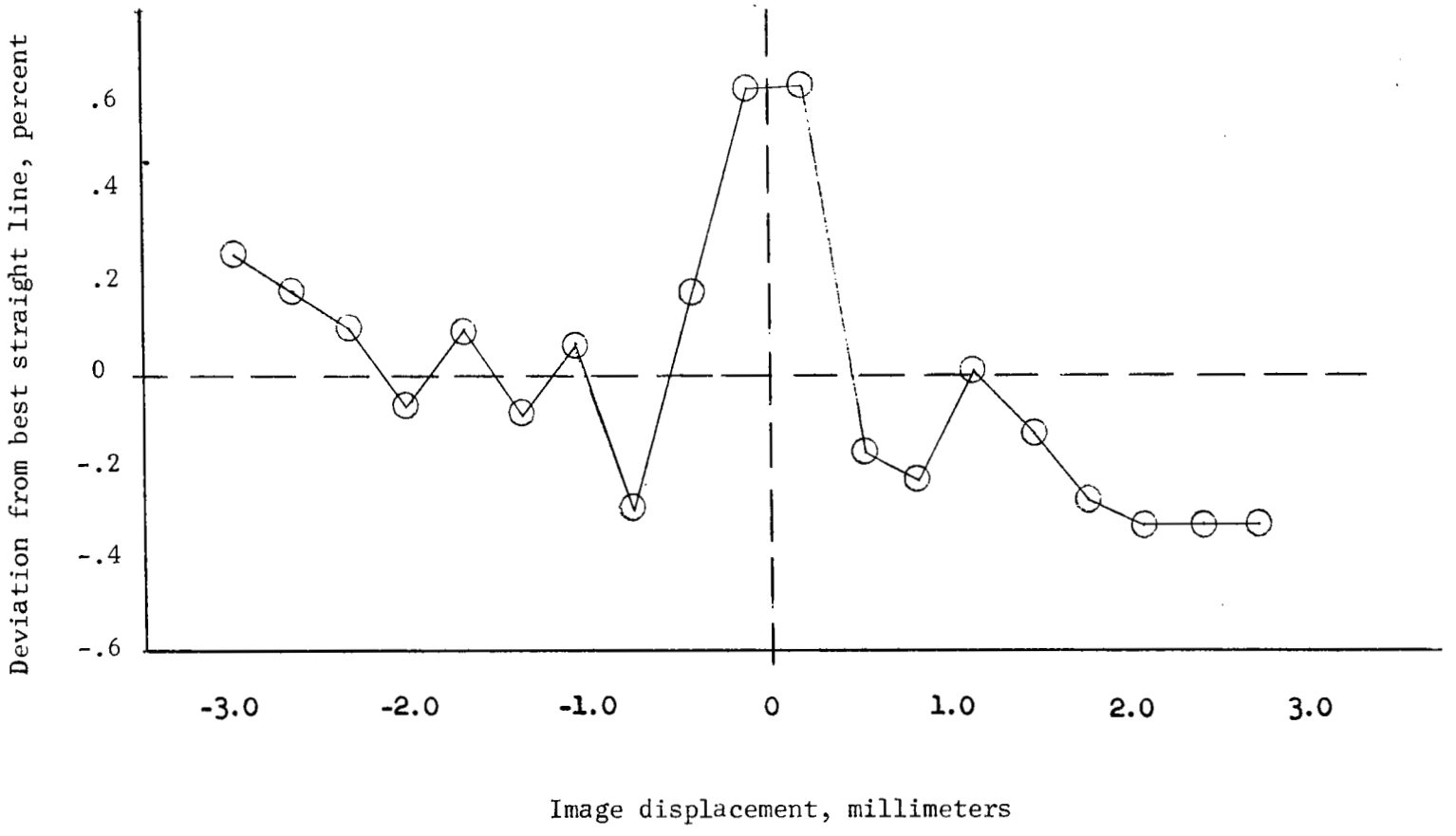

Figure 13.- Error in system linearity.

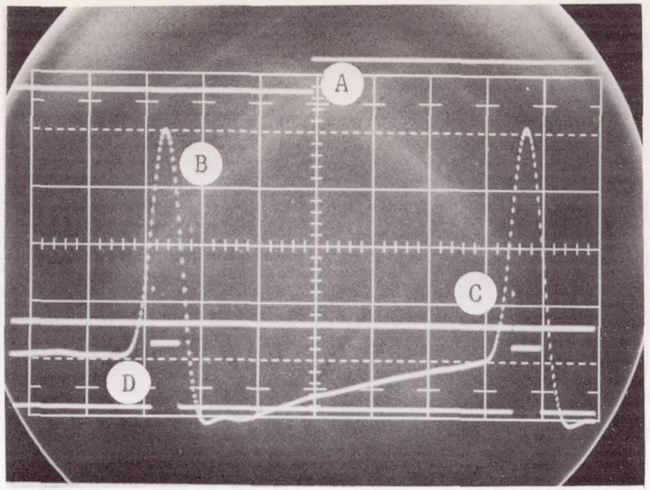

(a) 200 μsec/div.

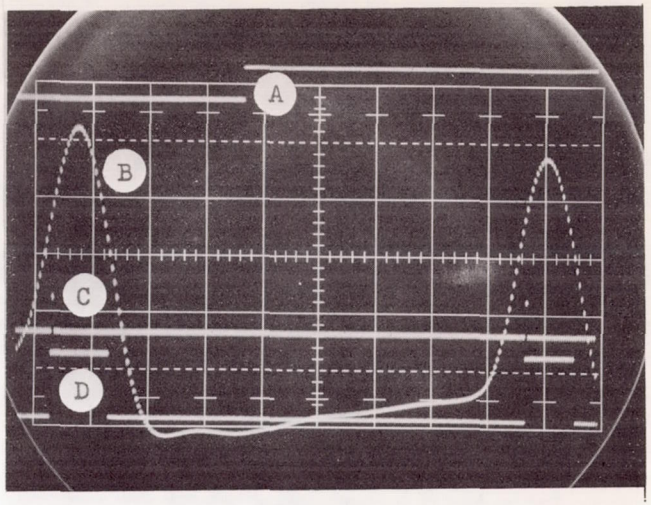

(b) 100 μsec/div.

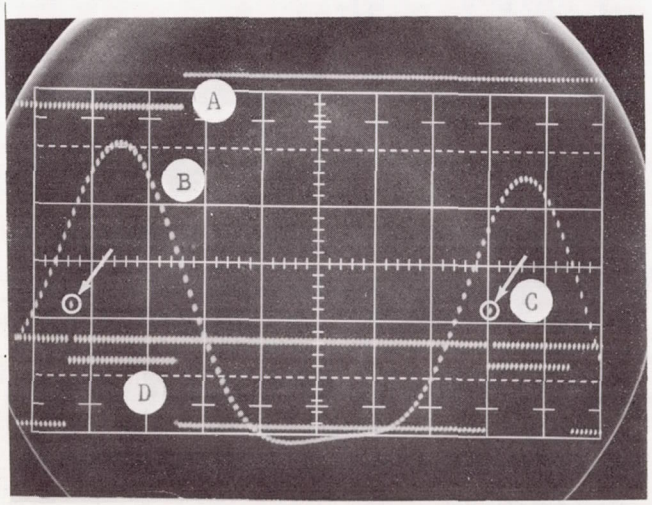

(c) 50 μsec/div.

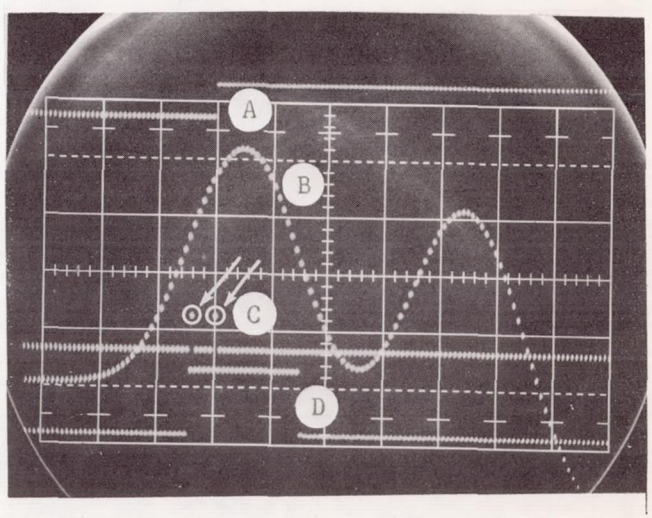

(d) 50 μsec/div.

Figure 14.- Typical signal at end points of sweep position. Star magnitude, 11.5; sweep frequency, 50 hertz.

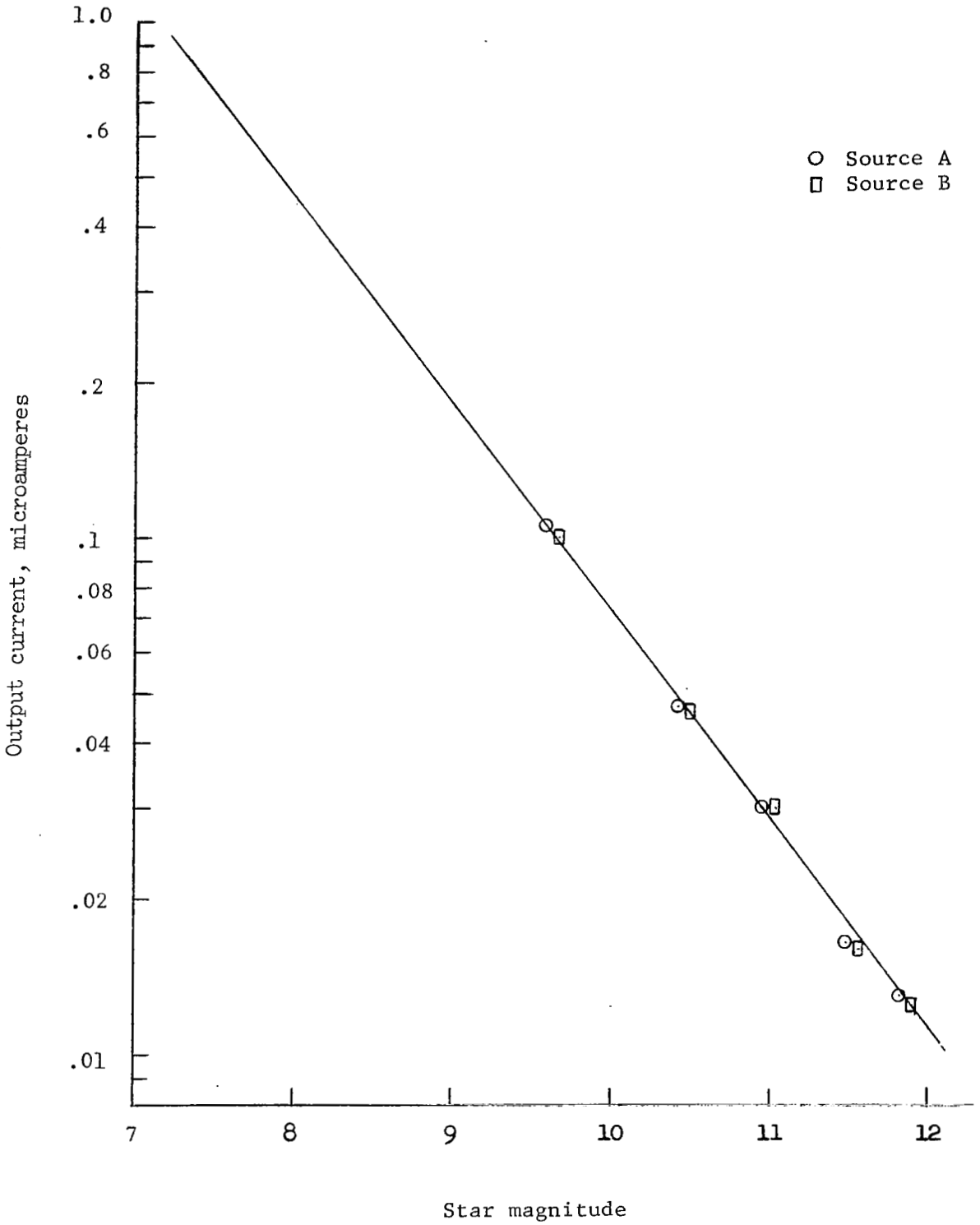

Figure 15.- Variation of image dissector current with star magnitude.

NASA-Langley, 1969 —— 14 L-6450

"The aeronautical and space activities of the United States shall be conducted so as to contribute . . . to the expansion of human knowledge of phenomena in the atmosphere and space. The Administration shall provide for the widest practicable and appropriate dissemination of information concerning its activities and the results thereof."

—NATIONAL AERONAUTICS AND SPACE ACT OF 1958

NASA SCIENTIFIC AND TECHNICAL PUBLICATIONS

TECHNICAL REPORTS: Scientific and technical information considered important, complete, and a lasting contribution to existing knowledge.

TECHNICAL NOTES: Information less broad in scope but nevertheless of importance as a contribution to existing knowledge.

TECHNICAL MEMORANDUMS: Information receiving limited distribution because of preliminary data, security classification, or other reasons.

CONTRACTOR REPORTS: Scientific and technical information generated under a NASA contract or grant and considered an important contribution to existing knowledge.

TECHNICAL TRANSLATIONS: Information published in a foreign language considered to merit NASA distribution in English.

SPECIAL PUBLICATIONS: Information derived from or of value to NASA activities. Publications include conference proceedings, monographs, data compilations, handbooks, sourcebooks, and special bibliographies.

TECHNOLOGY UTILIZATION PUBLICATIONS: Information on technology used by NASA that may be of particular interest in commercial and other non-aerospace applications. Publications include Tech Briefs, Technology Utilization Reports and Notes, and Technology Surveys.

Details on the availability of these publications may be obtained from:

SCIENTIFIC AND TECHNICAL INFORMATION DIVISION

NATIONAL AERONAUTICS AND SPACE ADMINISTRATION

Washington, D.C. 20546